IJAME
Int. J. of Applied Mechanics and Engineering, 2025, vol.30, No.4, pp.67-85
DOI: 10.59441/ijame/210540

PARAMETRIC ANALYSIS AND OPTIMIZATION OF WIRE EDM FOR IMPROVED SURFACE ROUGHNESS OF D2 TOOL STEEL USING RESPONSE SURFACE METHODOLOGY

D.P. Kharat* and M.P. Nawathe
Mechanical Engineering, Prof. Ram Meghe Institute of Technology & Research Badnera, INDIA
E-mail: kharatdipak18@gmail.com

This study presents a systematic investigation into the optimization of Wire Electrical Discharge Machining (WEDM) parameters for improving the surface finish of D2 tool steel. Utilizing Response Surface Methodology (RSM) integrated with Central Composite Design (CCD), the research aims to minimize surface roughness (*Ra*) through the controlled variation of critical process parameters: wire feed rate, pulse-on time, pulse-off time, peak current, and sensitivity. The optimal parameter configuration comprising a wire feed rate of *60 mm/min*, pulse-on time of *32* μs, pulse-off time of *7* μs, peak current of *4 A*, and sensitivity level of 5 resulted in a minimum surface roughness of approximately *3.7309* μm. These conditions enhanced process stability, facilitated efficient material removal, and reduced thermal damage, thereby preserving surface integrity. The developed regression model demonstrated high predictive accuracy, supported by a composite desirability index of *0.582*. Experimental validation confirmed the reliability and repeatability of the optimized parameter set. The findings underscore the significance of multi-parameter optimization in achieving high-precision surface characteristics, offering practical insights for advanced machining applications in tool and die manufacturing.

Key words: WEDM, D2 steel, surface roughness, response surface methodology, central composite design, optimization.

1. Introduction

WEDM is a non-conventional machining process that uses electrical discharges between a moving wire electrode and a conductive workpiece to precisely machine hard materials and intricate geometries. Since its inception in the 1960s, WEDM has become indispensable in precision-driven sectors such as aerospace, automotive, and medical device manufacturing due to its ability to produce complex shapes with exceptional accuracy and surface finish [1, 2]. The process performance is highly dependent on parameters like pulse-on time, pulse-off time, wire feed rate, and peak current, making their optimization essential for achieving high efficiency and accuracy [3]. Studies such as those by Babu *et al.* [4] have demonstrated the critical role of parameter optimization in improving material removal rate (MRR) and surface finish for materials like aluminum 6061. Advanced techniques, including Artificial Neural Networks (ANN) combined with Particle Swarm Optimization (PSO), have been successfully applied to enhance machining outcomes for difficult-to-machine alloys like Inconel 750 [5]. Similar optimization strategies have yielded notable improvements in surface roughness and MRR across stainless steel and other alloys [6]. The complexity of WEDM optimization, especially for advanced materials like Ti-6Al-4V, has led to the adoption of intelligent algorithms such as Teaching-Learning-Based Optimization (TLBO) to fine-tune process parameters [9]. Techniques like Grey Relational Analysis (GRA), often integrated with multi-objective optimization strategies, effectively balance trade-offs among key outputs such as MRR, surface roughness, and dimensional accuracy [10]. Recent developments in methods like RSM and Grey-based RSM have further enhanced parameter control, contributing to more consistent and precise machining outcomes [13]. These advancements are particularly significant when working with challenging materials such as superalloys and composites [14], and ongoing

* To whom correspondence should be addressed

research in sustainable and advanced optimization techniques continues to improve WEDM's efficiency, precision, and environmental compatibility [18, 19].

Parameter optimization in WEDM remains critical for achieving high-quality, energy-efficient machining, especially in precision-focused sectors like aerospace and medical device manufacturing. It not only ensures compliance with stringent quality standards but also minimizes waste and energy consumption. As newer and harder alloys emerge, the demand for optimized WEDM processes will intensify, making such advancements indispensable for maintaining competitiveness in high-tech manufacturing [20-22]. Continued research is essential to meet the evolving demands of modern industry, as reflected in recent literature covering advancements in optimization strategies and their practical applications [23-27, 28-35]. While WEDM is effective for hard materials like D2 steel–where achieving superior surface finish is crucial–few studies have focused on optimizing process parameters for this material. This work applies RSM to minimize surface roughness by optimizing wire feed, pulse timings, peak current, and sensitivity, thereby enhancing both machining quality and industrial applicability. Recent works have focused on nanoparticle-reinforced scaffolds, bio-nanocomposites, and the effect of process parameters on welding quality, surface properties, and metallurgical coatings for wear resistance and durability using such techniques [36-48].

2. Materials and methods

D2 tool steel was selected as the workpiece material due to its high hardness, wear resistance, and dimensional stability under stress, making it ideal for precision tool and die applications and well-suited for the thermal and mechanical demands of WEDM. Its chemical composition is provided in Tab.1. *A 0.25 mm* diameter brass wire, chosen for its superior electrical conductivity and spark stability, was employed as the cutting electrode to ensure accurate machining and enhanced surface finish on hard materials like D2 steel. WEDM experiments were conducted on a CNC WEDM system with advanced control capabilities, facilitating precise adjustment of critical parameters: wire feed rate, pulse-on time, pulse-off time, peak current, and sensitivity as show in Fig.1. Preliminary trials were performed to establish feasible parameter ranges and verify system reliability.

Table 1. Key compositional elements for D2 steel and brass wire.

Material/Composition (%)	(C)	(Cr)	(Mo)	(V)	(Mn)	(Si)	(P)	(S)	(Fe)
D2 Steel	*1.40*	*1*	*0.80*	*0.2*	*0.6*	*0.6*	*0.03*	*0.03*	Balance
Material/ Composition	(Cu)	(Zn)	(Pb)	(Sn)	(Fe)				
Brass Wire	*60*	*40*	*0.08*	*0.10*	*0.05*				

The initial testing phase was carefully designed to establish the feasible operating range of WEDM parameters for machining D2 tool steel using a brass wire electrode. The objective was to identify parameter settings significantly influencing surface roughness (*Ra*). Key variables Peak Current, Pulse On-Time, Pulse Off-Time, Wire Feed Rate, and Sensitivity were varied across three levels (Tab.2) to assess their impact on surface quality. After each run, the workpiece was extracted and analyzed for surface finish and process stability. Surface roughness was measured using a high-precision profilometer to ensure data accuracy. Observations on process behavior and parameter effects were systematically recorded.

The parameter ranges (Tab.2), established from literature, prior studies, and preliminary trials, formed the basis for optimizing WEDM conditions on D2 steel. Five key inputs wire feed rate, pulse-on time, pulse-off time, peak current, and sensitivity were varied using a face-centered CCD with 32 runs (factorial, center, and axial points). Surface roughness (*Ra*) was measured in micrometers with a precision profilometer, using multiple readings and triplicate tests for accuracy. Specimens (*20×20×20 mm*) were cut from a D2 steel plate following a grid layout (Fig.2) and coded for traceability.

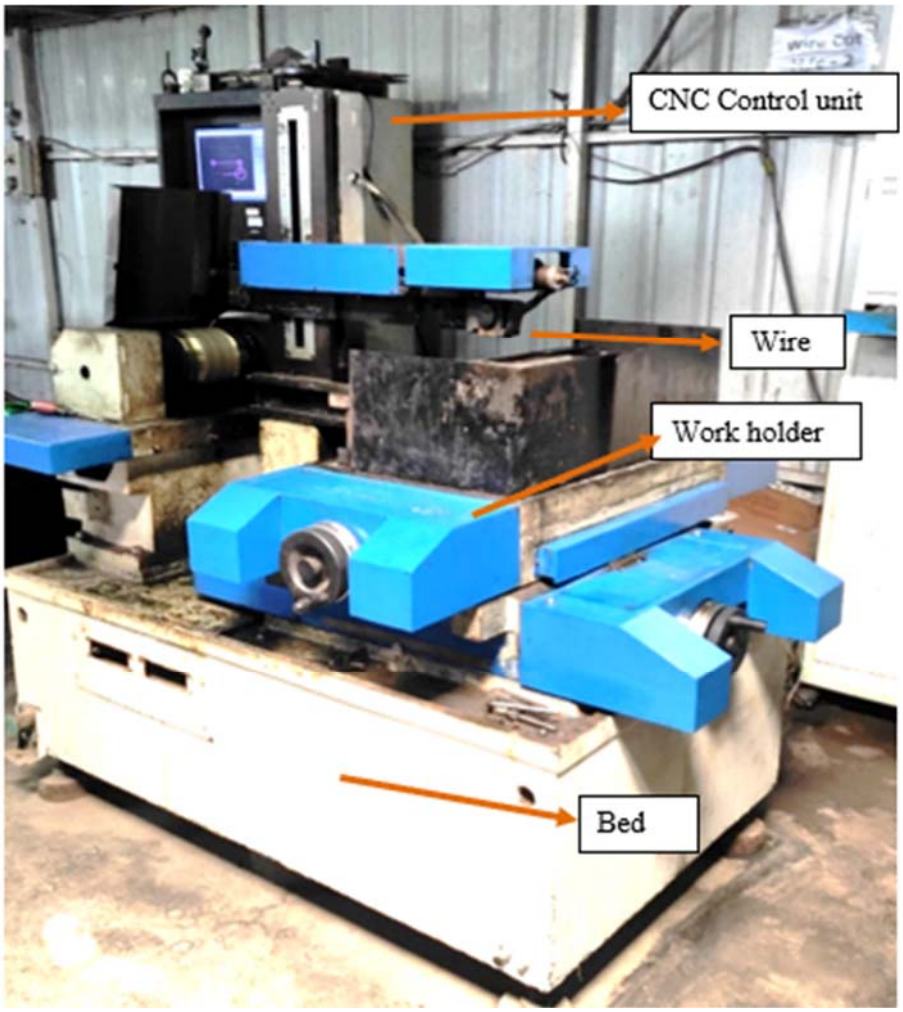

Fig.1. CNC WEDM system for experimental set up.

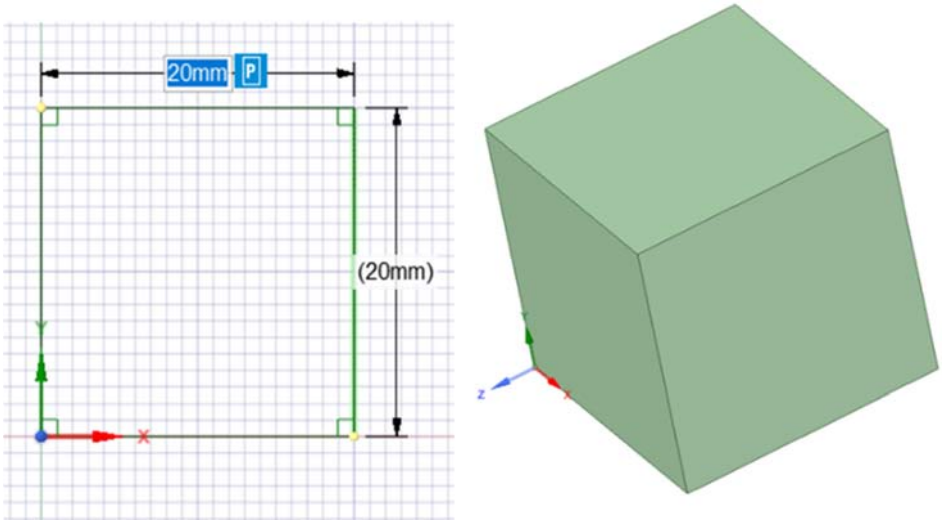

Fig.2. Plan of specimen preparation as per DOE.

Table 2. Workable ranges of main influencing machining parameters

Sr. No.	Parameters	Unit	Level 1	Level 2	Level 3
1	Wire feed rate F	*mm/min*	*60*	*75*	*90*
2	Pulse on-time T_{on}	μ*s*	*32*	*37*	*42*
3	Pulse off-time T_{off}	μ*s*	*4*	*5.5*	*7*
4	Peak current P	*A*	*2*	*3*	*4*
5	Sensitivity S	Unit less	*5*	*7.5*	*10*

3. Results and discussion

Table 4 summarizes the ANOVA results for the regression model, providing key insights into the WEDM process. The model demonstrates strong statistical significance (F-value = *930.08*, P-value = *0.000*), indicating that the selected factors significantly affect *Ra*. The linear terms confirm that each parameter, such as wire feed rate and pulse-on time, independently contributes to the response. Additionally, the square term reveals a significant quadratic effect for wire feed rate, suggesting a non-linear relationship with *Ra*. The 2-way interaction terms imply that interactions between at least two parameters significantly influence the outcome. The model's robustness is reinforced by its excellent goodness-of-fit metrics: an R-squared of *99.83%* indicates that nearly all variability in *Ra* is explained by the model, while the adjusted R-squared of *99.72%* (Tab.5) confirms this is not due to overfitting. Moreover, the predicted R-squared of *99.48%* highlights the model's strong generalization capability for new data. These results collectively affirm the model's reliability and effectiveness in modeling the complex parameter-response relationships in WEDM. The corresponding regression equation for *Ra* (SR) is provided in Eq.(3.1).

Regression equation for *Ra* (SR):

$$\begin{aligned} Ra = {} & 7.92 - 0.0987 \cdot A - 0.0550 \cdot B - 0.1737 \cdot C + 0.0373 \cdot D - 0.013 \cdot E + 0.0007 \cdot A \cdot A + \\ & + 0.00034 \cdot A \cdot B - 0.00047 \cdot A \cdot C - 0.00018 A \cdot E + 0.007 \cdot C \cdot C + 0.0014 \cdot B \cdot E - 0.007 \cdot C \cdot D \end{aligned} \tag{3.1}$$

where,

Ra = surface roughness, A = wire feed rate *mm/min*, B = pulse on time T_{on},

C = pulse of time T_{off}, D = peak current A, E = sensitivity.

Table 3. Design of experiment using RSM with measured responses.

Sr. No.	*F mm/min*	T_{on} μ*s*	T_{off} μ*s*	*P A*	*S*	*Ra* μ*m*
1	*90*	*42*	*4*	*2*	*10*	*4.600*
2	*75*	*37*	*5.5*	*3*	*7.5*	*4.015*
3	*90*	*37*	*5.5*	*3*	*7.5*	*4.500*
4	*75*	*37*	*5.5*	*3*	*7.5*	*4.015*
5	*75*	*37*	*5.5*	*4*	*7.5*	*4.045*
6	*75*	*32*	*5.5*	*3*	*7.5*	*3.915*
7	*90*	*32*	*7*	*4*	*5*	*4.281*
8	*90*	*42*	*4*	*4*	*5*	*4.460*
9	*75*	*42*	*5.5*	*3*	*7.5*	*4.115*
10	*90*	*32*	*4*	*2*	*5*	*4.340*

Table 3cont. Design of experiment using RSM with measured responses.

Sr. No.	*F mm/min*	T_{on} μs	T_{off} μs	*P A*	*S*	*Ra* μm
11	*90*	*42*	*7*	*2*	*5*	*4.620*
12	*60*	*37*	*5.5*	*3*	*7.5*	*3.864*
13	*60*	*42*	*7*	*2*	*10*	*4.160*
14	*90*	*32*	*7*	*2*	*10*	*4.390*
15	*60*	*42*	*7*	*4*	*5*	*3.930*
16	*75*	*37*	*5.5*	*3*	*7.5*	*4.015*
17	*75*	*37*	*5.5*	*3*	*10*	*4.085*
18	*60*	*32*	*7*	*4*	*10*	*3.840*
19	*60*	*32*	*4*	*4*	*5*	*3.760*
20	*75*	*37*	*7*	*3*	*7.5*	*4.075*
21	*90*	*32*	*4*	*4*	*10*	*4.440*
22	*75*	*37*	*5.5*	*3*	*5*	*3.929*
23	*60*	*32*	*7*	*2*	*5*	*3.761*
24	*60*	*32*	*4*	*2*	*10*	*3.860*
25	*75*	*37*	*5.5*	*2*	*7.5*	*3.985*
26	*75*	*37*	*5.5*	*3*	*7.5*	*4.015*
27	*90*	*42*	*7*	*4*	*10*	*4.750*
28	*75*	*37*	*5.5*	*3*	*7.5*	*4.015*
29	*60*	*42*	*4*	*4*	*10*	*3.940*
30	*75*	*37*	*4*	*3*	*7.5*	*3.973*
31	*60*	*42*	*4*	*2*	*5*	*3.760*
32	*75*	*37*	*5.5*	*3*	*7.5*	*4.015*

Table 4. Analysis of variance.

Source	DF	Adj SS	Adj MS	F-Value	P-Value
Model	*12*	*2.241*	*0.186*	*930.08*	*0.000*
Linear	*5*	*1.962*	*0.392*	*1954.01*	*0.000*
F	*1*	*1.684*	*1.684*	*8384.73*	*0.000*
T_{on}	*1*	*0.169*	*0.169*	*845.08*	*0.000*
T_{off}	*1*	*0.025*	*0.025*	*125.64*	*0.000*
P	*1*	*0.000*	*0.000*	*0.25*	*0.624*
S	*1*	*0.083*	*0.083*	*414.36*	*0.000*
Square	*1*	*0.216*	*0.216*	*1077.03*	*0.000*
$F \cdot F$	*1*	*0.216*	*0.216*	*1077.03*	*0.000*
2-Way Interaction	*6*	*0.063*	*0.010*	*52.32*	*0.000*
$F \cdot T_{on}$	*1*	*0.010*	*0.010*	*52.30*	*0.000*
$F \cdot T_{off}$	*1*	*0.001*	*0.001*	*8.99*	*0.007*
$F \cdot S$	*1*	*0.000*	*0.000*	*3.76*	*0.067*
$T_{on} \cdot T_{off}$	*1*	*0.042*	*0.042*	*213.32*	*0.000*
$T_{on} \cdot S$	*1*	*0.005*	*0.005*	*26.53*	*0.000*

Table 4cont. Analysis of variance.

$T_{off} \cdot P$	*1*	*0.001*	*0.001*	*8.99*	*0.007*
Error	*19*	*0.003*	*0.000*		
Lack-of-Fit	*14*	*0.003*	*0.000*		
Pure Error	*5*	*0.000*	*0.000*		
Total	*31*	*2.245*			

Table 5. Model summary.

S	*R*-sq	*R*-sq (adj)	*R*-sq (pred)
0.0141728	*99.83%*	*99.72%*	*99.48%*

3.1. Effect of process parameters

Figure 3 presents the main effects plot, which is used to evaluate the individual influence of each Wire EDM parameter on the surface roughness (*Ra*) of D2 tool steel. This plot displays the average response of *Ra* at different levels of each factor while maintaining the other parameters at their central levels, allowing the isolated impact of each factor to be analyzed effectively. The observed results of each parameter are:

1. Wire Feed Rate (*mm/min*): A distinct non-linear trend is observed. Surface roughness (*Ra*) decreases significantly as the wire feed rate increases from *60 mm/min* to *75 mm/min*, indicating improved surface quality. This improvement is attributed to better flushing of molten material and debris from the spark gap, preventing re-deposition on the surface. However, beyond *75 mm/min*, *Ra* slightly increases. This is likely due to instability in the sparking process caused by excessive wire movement, which reduces spark density and energy concentration, thereby degrading surface finish. At very low feed rates, the wire dwells longer at a location, concentrating spark energy and generating larger craters, thus increasing *Ra*.
2. Pulse On Time (T_{on} , μs): A positive correlation between T_{on} and *Ra* is evident. As T_{on} increases, the duration of electrical discharge per pulse becomes longer, which allows more thermal energy to be transferred to the workpiece. This results in the formation of deeper and wider craters on the surface, thereby increasing surface roughness. Conversely, shorter pulse on times reduces the energy per spark, limiting crater size and yielding a finer surface finish due to more controlled erosion and lower thermal stress.
3. Pulse Off Time (T_{off} , μs): An increase in T_{off} leads to a slight reduction in *Ra*. Longer off times allow more effective flushing of eroded debris from the inter-electrode gap and enable the workpiece to cool between discharges. This reduces secondary discharges and re-deposition of molten material, which contributes to smoother surfaces. However, excessively long T_{off} may adversely affect the overall machining efficiency by reducing the frequency of sparking events, hence a balance must be maintained.
4. Peak Current (*A*): The effect of peak current on *Ra* appears to be minimal within the tested range. This suggests that, under the experimental conditions, the thermal energy associated with the current did not vary enough to produce a significant change in crater morphology or surface roughness. It may also imply that current-related effects are overshadowed by more dominant factors such as T_{on} and wire feed rate in determining surface texture.
5. Sensitivity: A rising trend is observed in *Ra* with increasing sensitivity. Sensitivity in Wire EDM relates to the machine's responsiveness to changes in gap conditions. Higher sensitivity settings may cause erratic spark initiation and unstable discharge conditions, leading to inconsistent material removal and localized overheating. This contributes to an uneven surface texture and increased *Ra*. In

contrast, lower sensitivity settings promote a more uniform discharge regime, allowing for smoother and more predictable erosion, thereby reducing surface roughness.

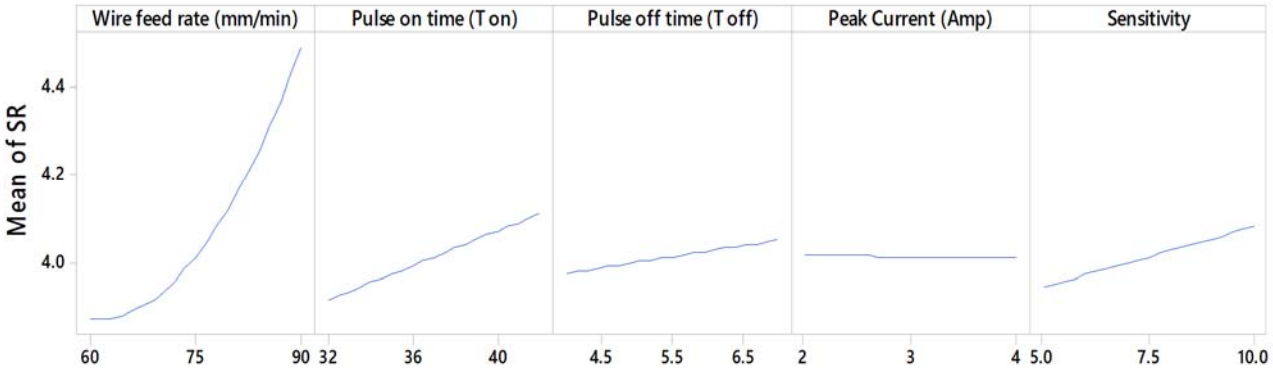

Fig.3. Main effects plot for *Ra*.

The main effects plot visually identifies key parameters and their optimal ranges for minimizing *Ra*. However, interactions between factors require further analysis through interaction plots, as shown in Fig.4. Figure 4 presents the interaction plots for surface roughness (*Ra*), offering insights into how the combined effects of different Wire EDM parameters influence the machining outcome. While the main effects plot identifies the individual impact of each parameter, interaction plots are crucial in revealing how the response (*Ra*) changes when two parameters are varied simultaneously. Non-parallel or intersecting lines in these plots indicate the presence of interaction effects–meaning the influence of one parameter on *Ra* is dependent on the level of another parameter. The interaction plot reveals how factors influence *Ra* through their combined effects:

1. Wire Feed Rate and Pulse on Time: The distinctly non-parallel lines in this plot confirm a strong interaction between wire feed rate and pulse on time. A combination of higher wire feed rates and shorter pulse durations leads to lower *Ra* values. Physically, this is due to the improved debris removal and reduced thermal energy per spark, which results in finer craters. At lower feed rates, longer pulse durations cause excessive localized heating, leading to larger craters and rougher surfaces. Thus, the interplay between feed rate and pulse energy duration critically affects surface quality.
2. Wire Feed Rate and Pulse Off Time: The slightly non-parallel lines here suggest a moderate interaction. A slower wire feed rate combined with a longer pulse off time tends to produce smoother surfaces. This is attributed to enhanced cooling and better flushing of molten material when the spark frequency is reduced (due to longer T_{off}), especially at lower wire speeds where debris accumulation is more likely. However, the interaction is not as pronounced as in the previous case, indicating that T_{off} has a more independent effect on *Ra* when combined with wire feed.
3. Pulse on Time and Pulse Off Time: The intersecting lines clearly indicate a significant interaction. A combination of shorter pulse on time and longer pulse off time yields the lowest surface roughness. Physically, this reflects an optimal thermal balance–shorter T_{on} reduces the energy input per discharge, minimizing crater size, while longer T_{off} facilitates cooling and debris evacuation, preventing secondary discharges or redeposition. The interaction suggests that optimizing these two-timing parameters together is essential for achieving a fine surface finish.
4. Peak Current Interactions (with Wire Feed Rate, T_{on}, and T_{off}): The near-parallel nature of lines involving peak current indicates negligible interaction effects with the other process parameters. This implies that within the tested range, peak current has a relatively consistent and limited impact on *Ra* regardless of changes in wire feed, T_{on}, or T_{off}. This might be due to the narrow current range used

or the fact that other parameters have a more dominant role in determining the discharge energy and resulting surface topography.

5. Sensitivity Interactions (with Wire Feed Rate, T_{on}, and T_{off}): The non-parallel lines in these interaction plots indicate that sensitivity interacts notably with other parameters. Lower sensitivity settings generally produce smoother surfaces, particularly when combined with higher wire feed rates and shorter T_{on}/T_{off} durations. From a physical standpoint, high sensitivity can lead to unstable gap control and erratic spark generation, which adversely affects surface finish. Conversely, lower sensitivity stabilizes the discharge process, especially when combined with parameter settings that already promote uniform spark distribution, thereby improving *Ra*.

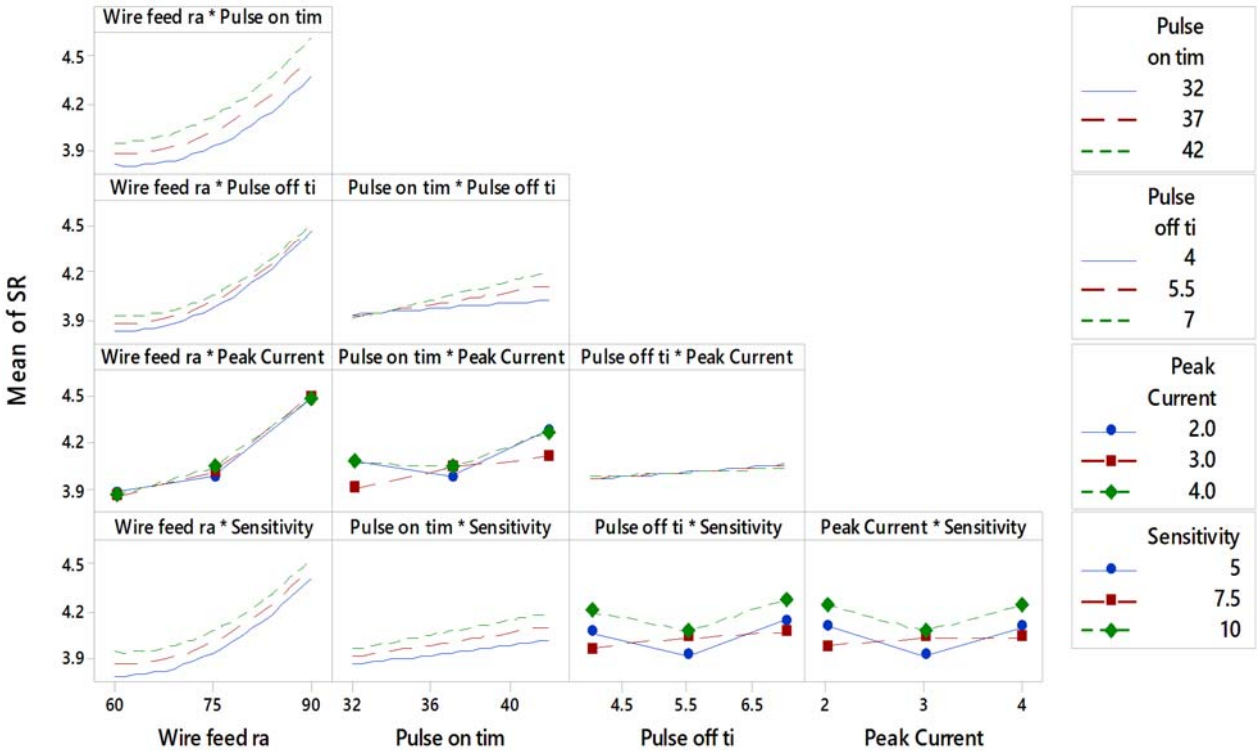

Fig.4. Interaction plots of all considered process parameters for *Ra*.

Interaction plots are useful for identifying the presence and nature of interaction effects between factors. In this case, the plots indicate significant interactions among wire feed rate, pulse on time, pulse off time, and sensitivity, while interactions involving peak current appear minimal or negligible.

3.2. Analysis using response surface graph

Figure 5 illustrates a three-dimensional (3D) response surface plot depicting the combined influence of sensitivity and peak current on surface roughness (*Ra*), with other parameters–wire feed rate (*75 mm/min*), pulse on time ($T_{on} = 37\mu s$), and pulse off time ($T_{off} = 5.5\mu s$)–held constant. The *x*-axis represents peak current (*2-4 A*), the *y*-axis represents sensitivity (*5-10*), and the *z*-axis shows the resulting *Ra* values.

1. Effect of Sensitivity on *Ra*: The response surface demonstrates a pronounced upward gradient along the sensitivity axis, indicating that *Ra* increases with increasing sensitivity. Physically, higher sensitivity settings make the servo control system more reactive to minor fluctuations in the inter-

electrode gap, often resulting in unstable and erratic discharge conditions. This can lead to uneven material erosion and localized overheating, which contribute to increased surface roughness. In contrast, lower sensitivity settings stabilize the discharge process, allowing for more uniform material removal and producing smoother surface finishes. This trend corroborates observations from the main effects and interaction plots.

2. Effect of Peak Current on *Ra*: The surface shows relatively minimal variation in *Ra* along the peak current axis, suggesting that within the tested range (*2-4 A*), peak current exerts a weak influence on surface roughness. This can be attributed to the narrow range of current levels explored, where the energy per discharge did not vary sufficiently to significantly alter crater morphology or surface texture. In this regime, the thermal load delivered to the workpiece may be too moderate to cause pronounced changes in *Ra*, especially when other parameters dominate the spark energy behavior (e.g., T_{on} and sensitivity).
3. Interaction Between Sensitivity and Peak Current: The 3D surface appears relatively flat and lacks significant curvature or slope variation in regions where, sensitivity and peak current change simultaneously. This flatness indicates a weak or negligible interaction effect between sensitivity and peak current. In other words, the effect of sensitivity on *Ra* is largely independent of the peak current setting, and vice versa. This aligns with the interaction plots, which showed near-parallel lines for peak current in combination with other factors, confirming its limited contribution to the variation in *Ra* under the given experimental conditions.

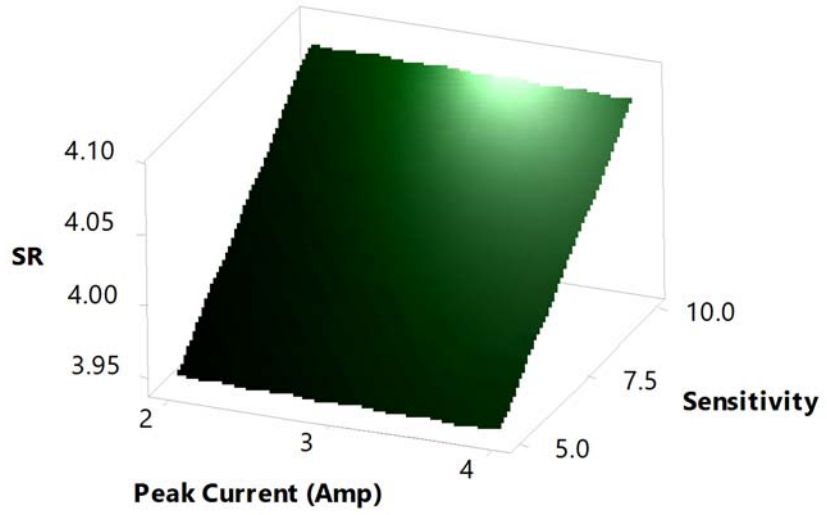

Fig.5. Response graph of *Ra* verses sensitivity and peak current.

Figure 6 illustrates the 3D surface plot showing the interactive effect of sensitivity and pulse-off time T_{off} on surface roughness (*Ra*). In this plot, T_{off} is represented on the *x*-axis, sensitivity on the *y*-axis, and *Ra* on the *z*-axis. The other machining parameters were held constant: wire feed rate at *75 mm/min*, pulse-on time at *37* μ*s*, and peak current at *3 A*. The surface morphology reveals that *Ra* reaches a maximum of approximately *4.1* μ*m* when both sensitivity and T_{off} are at their lowest levels (in the range of *5-6*). This region corresponds to inefficient flushing and unstable discharge conditions. As both sensitivity and T_{off} increase, a notable reduction in *Ra* is observed–highlighted by the downward gradient of the surface toward the green region. This behavior can be explained by the following physical mechanisms:

1. Sensitivity influences the feedback control in maintaining the spark gap. At low sensitivity settings, the control system reacts slowly to gap variations, leading to erratic sparking and inconsistent material

removal. Increasing sensitivity enhances spark stability and allows for more uniform erosion, thereby improving surface quality.

2. Pulse-off time T_{off} governs the duration between consecutive discharges. At low T_{off}, insufficient time is allowed for the dielectric to recover and for molten debris to be flushed out of the gap, increasing the likelihood of arcing and re-deposition. As T_{off} increases, the inter-spark gap clears more effectively and the workpiece cools adequately, promoting finer surface finishes.

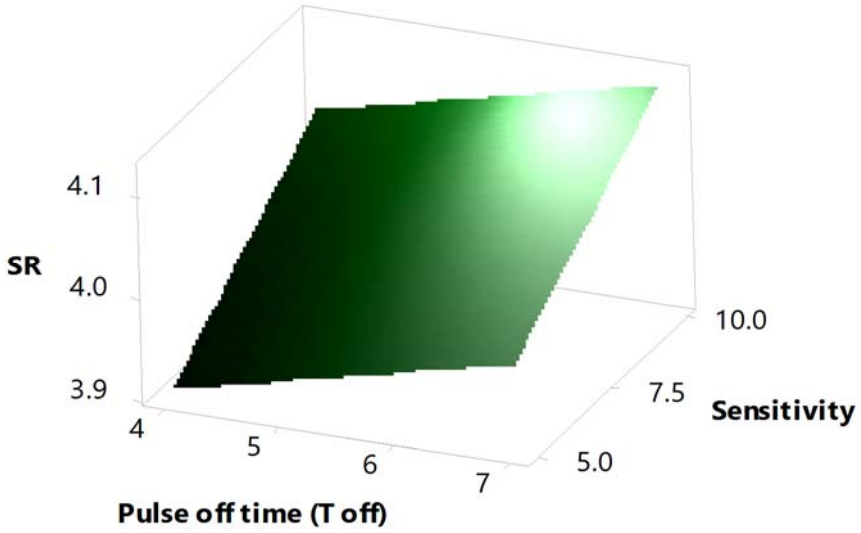

Fig.6. Response graph of *Ra* versus sensitivity and T_{off}.

Figure 7 presents another surface plot depicting the interaction between peak current and pulse-off time T_{off} on *Ra*. In this case, T_{off} is on the *x*-axis, peak current on the *y*-axis, and *Ra* on the *z*-axis. The constant parameters are wire feed rate (*75 mm/min*), pulse-on time (*37* μ*s*), and sensitivity (set value not varied here). The plot shows that the surface roughness peaks at approximately *4.05* μ*m* when both peak current (around *2 A*) and T_{off} (*4-5* μ*s*) are at lower levels. However, with increasing peak current and T_{off}, *Ra* drops significantly, as evidenced by the steep downward slope of the surface in the green region. This trend is primarily due to the following reasons:

1. Peak Current: While higher peak current increases the energy per spark and leads to more aggressive material melting, it can also improve surface finish under controlled conditions. The molten material is more completely removed due to enhanced vaporization and effective flushing, resulting in smoother crater profiles. However, this effect is only beneficial if the discharge energy does not exceed the stability threshold, beyond which surface roughness would increase again due to over-melting or micro-cracking.
2. Pulse-off Time T_{off}: As previously noted, increased T_{off} enhances cooling and flushing efficiency. It allows the dielectric fluid to re-ionize and stabilizes the gap condition, which contributes to a more uniform erosion pattern. This controlled thermal cycle prevents the formation of irregular recast layers and reduces surface defects, leading to improved *Ra*.

The 3D surface plot in Fig.8 demonstrates the relationship between surface roughness (*Ra*), sensitivity, and pulse-on time (T_{on}). *Ra* attains its highest value, around *4.2* μ*m*, when both sensitivity and T_{on} are at their lowest levels. As these parameters increase, *Ra* decreases, evidenced by the downward sloping green region toward the plot's back-right corner. Physically, this can be explained by the increased sensitivity enhancing

the energy input during sparking, which promotes more melting and re-melting of the workpiece surface, leading to smoother craters and thus lower *Ra*. Similarly, longer pulse-on times extend the spark duration, increasing thermal energy delivered to the surface, which causes greater melting and plastic deformation, effectively smoothing surface asperities and reducing *Ra*.

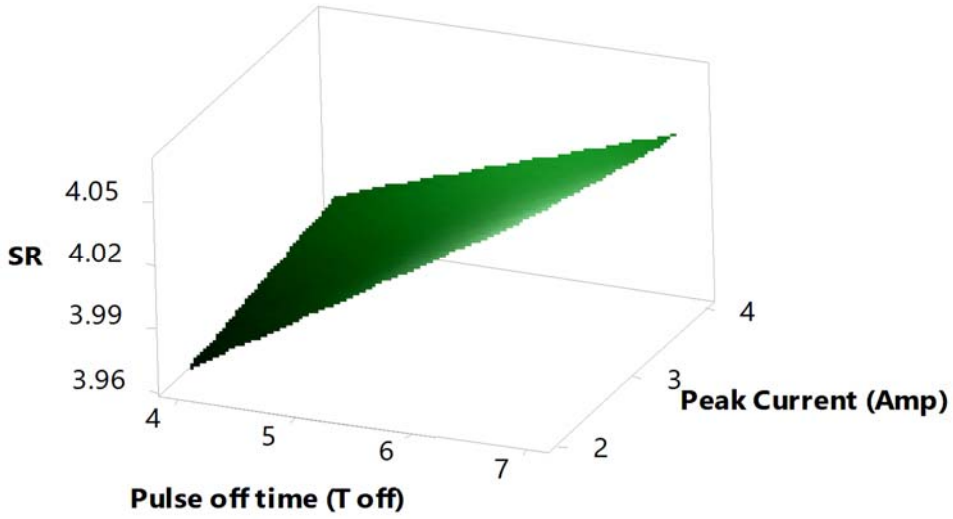

Fig.7. Response graph of *Ra* vs peak current and T_{off} .

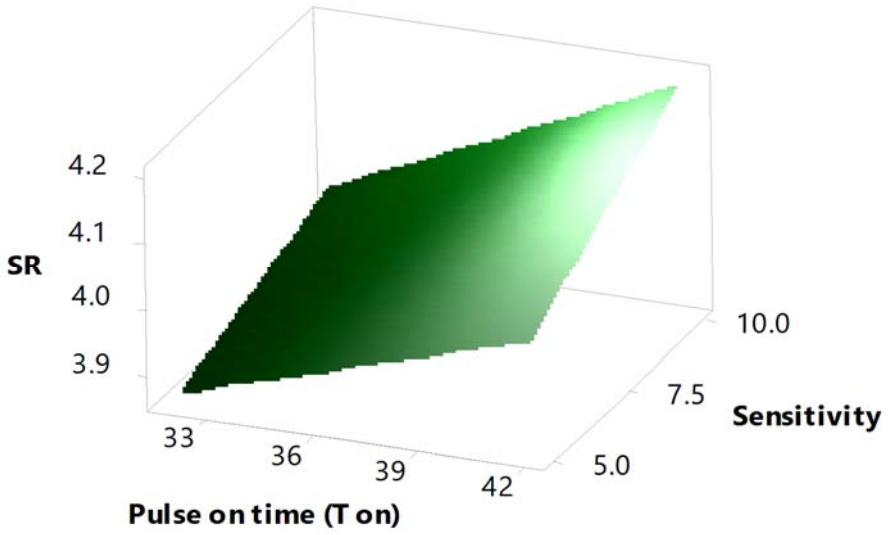

Fig.8. Response graph of *Ra* versus sensitivity and T_{on}

Figure 9 extends this analysis by illustrating the interaction of *Ra* with peak current and pulse-on time. *Ra* peaks near *4.10* μ*m* when both peak current and T_{on} are minimal, then decreases significantly as either parameter increases. Higher peak currents intensify the discharge energy, promoting greater melting and erosion of material peaks, which contributes to a more uniform surface texture and reduced *Ra*. Longer pulse-on times maintain the spark for extended periods, allowing sufficient thermal energy to smooth out irregularities caused by prior discharges. However, these improvements depend on maintaining optimal energy balance; excessive heat input can eventually lead to surface damage.

In Fig.10, the interplay between pulse-off time T_{off} and T_{on} is depicted, showing a maximum *Ra* (*~4.2* μ*m*) when both times are low. Increasing these durations reduces *Ra*, as longer T_{off} allows the dielectric fluid to flush away debris and cool the workpiece surface, preventing unstable arcs and localized overheating. Nevertheless, excessively long T_{off} can accelerate solidification rates, potentially causing surface defects such as micro-cracks or recast layers. Concurrently, longer T_{on} increases the total energy delivered per pulse, promoting melting and smoothing, but also risking thermal distortion if too high.

Figure 11 reveals the combined effect of sensitivity and wire feed rate on *Ra*, with *Ra* increasing as both parameters rise. Higher sensitivity enhances the servo control's responsiveness, potentially leading to more aggressive energy application and erratic sparking, which raises surface roughness. Increasing wire feed rate raises machining throughput, but also introduces turbulent flushing conditions and reduced spark stability, which can degrade surface quality.

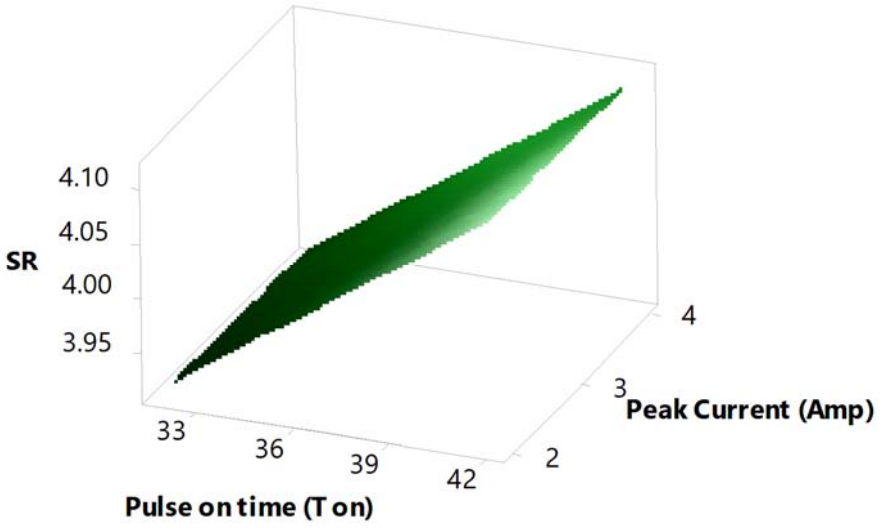

Fig.9. Response graph of *Ra* versus sensitivity and peak current.

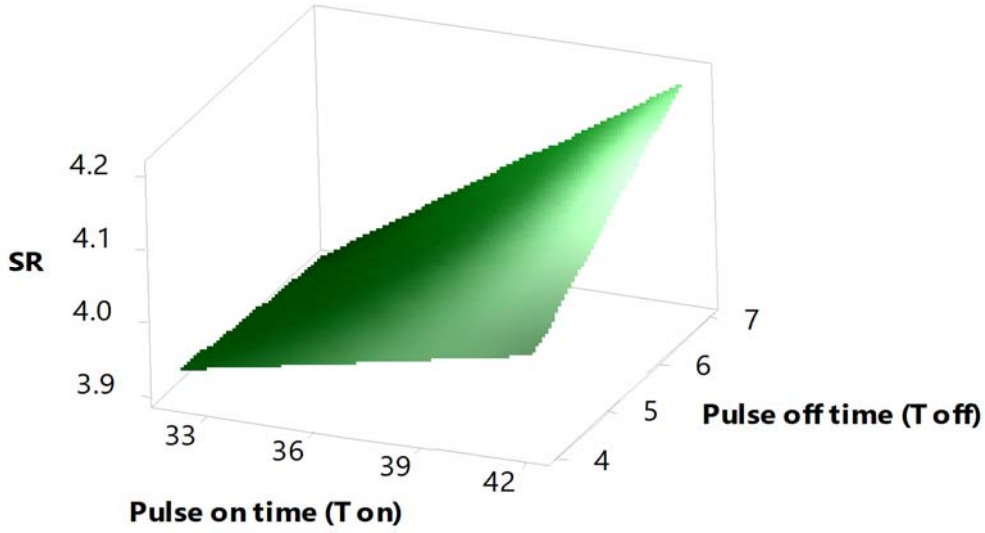

Fig.10. Response graph of *Ra* versus T_{off} and T_{on}.

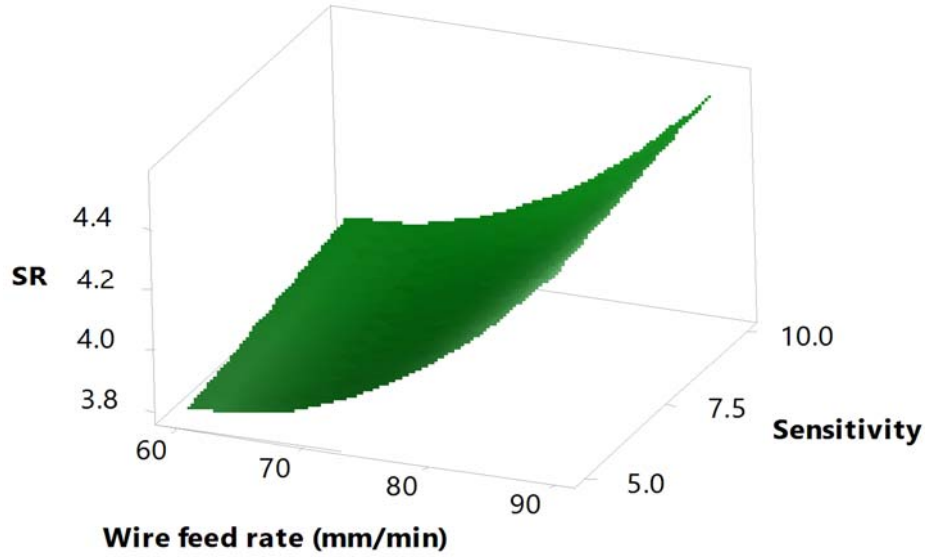

Fig.11. Response graph of *Ra* versus sensitivity and wire feed rate.

Figures 12 and 13 further detail these effects. Figure 12 shows a clear upward trend in *Ra* with increasing peak current (*2-4 A*) and wire feed rate (*60-90 mm/min*). Elevated peak currents increase discharge energy, intensifying material removal but causing rougher surfaces due to larger and deeper craters. Likewise, higher wire feed rates may improve productivity but also disrupt stable spark conditions, resulting in increased surface irregularities. Figure 13 illustrates how *Ra* varies with pulse-off time and wire feed rate: *Ra* rises with increasing T_{off}, likely due to prolonged cooling periods causing rapid solidification and microstructural defects, while wire feed rate influences *Ra* nonlinearly–initially decreasing *Ra* at lower feed rates (due to effective debris removal) before increasing it at higher rates where unstable sparking becomes dominant. The effect of feed rate is most pronounced at lower T_{off} values, suggesting that the electrical and mechanical parameters interact complexly to affect surface finish.

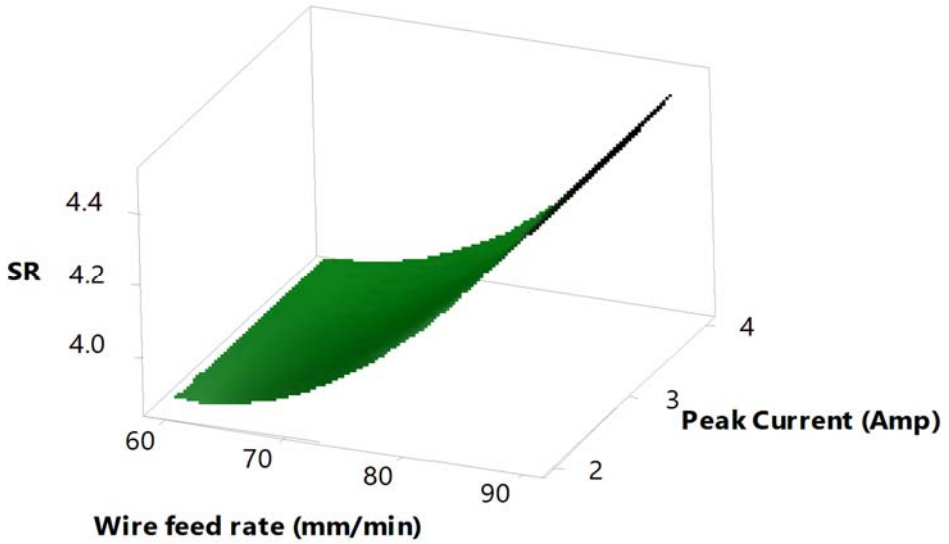

Fig.12. Response graph of *Ra* VS Peak Current and wire feed rate

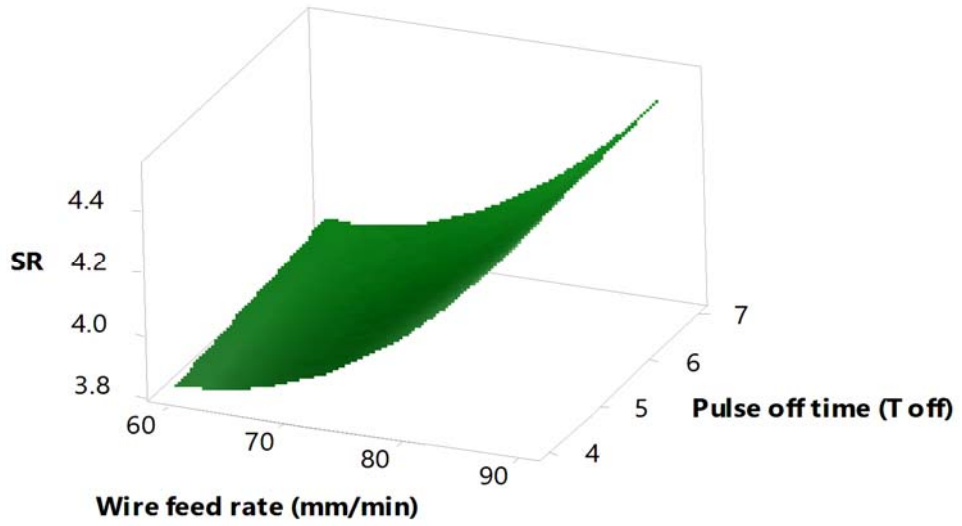

Fig.13. Response graph of *Ra* versus T_{off} and wire feed rate.

Finally, Fig.14 shows the interaction between pulse-on time and wire feed rate on *Ra*. *Ra* increases with longer T_{on}, peaking near *4.2* μ*s*, as extended pulse durations deliver more heat, enhancing melting but risking thermal damage. At lower T_{on}, *Ra* decreases initially with increasing wire feed rate, forming a valley at mid-range feed rates–this likely reflects an optimal balance where improved flushing and spark stability reduce roughness. Beyond this optimal feed rate, *Ra* rises again due to increased sparking instability. At higher T_{on}, *Ra* steadily increases with feed rate, suggesting that excessive thermal input combined with high feed rates exacerbates surface irregularities. These observations highlight that the interaction between electrical energy input and mechanical flushing rates critically governs surface quality in WEDM. Together, these figures underscore the intricate balance between process parameter pulse duration, current, sensitivity, and wire feed rate that determines the surface morphology of D2 tool steel in WEDM. The thermal and electrical dynamics influence melting, solidification, and material removal mechanisms, collectively shaping the final surface roughness and quality.

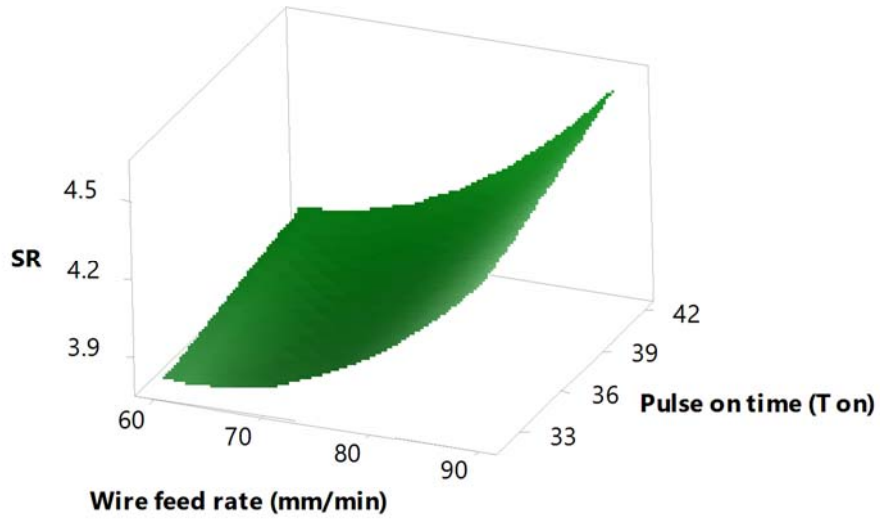

Fig.14. Response graph of *Ra* versus T_{on} and wire feed rate.

4. Optimization

The primary objective of the optimization was to reduce surface roughness (SR) within the target range of *3* to *4.75*, assigning equal weight to all process parameters. Wire feed rate was varied from *60-90 mm/min*, pulse on time from *32-42* µ*s*, pulse off time from *4-7* µ*s*, peak current from *2-4 A*, and sensitivity from *5-10*. Using RSM, the optimal settings were determined as: wire feed rate at *60 mm/min*, pulse on time at *32* µ*s*, pulse off time at *7* µ*s*, peak current at *4 A*, and sensitivity at *5*. These yielded a predicted *Ra* of *3.7309* with a composite desirability of *0.582*, indicating moderate optimization effectiveness due to trade-offs among parameters. The model demonstrated high accuracy, with a standard error of *0.0119*, a *95%* confidence interval of *3.7060-3.7559*, and a prediction interval of *3.6921-3.7697*. These narrow intervals confirm the robustness and precision of the model. The optimal configuration suggests setting wire feed rate, pulse on time, and sensitivity at their lower limits, and pulse off time and peak current at their upper limits–conditions favorable for minimizing SR. The moderate desirability score suggests that optimization was constrained by limited parameter ranges and potential nonlinear interactions, indicating that further refinement or advanced techniques may yield better outcomes. Figure 15 supports these findings by illustrating the influence of each parameter on SR.

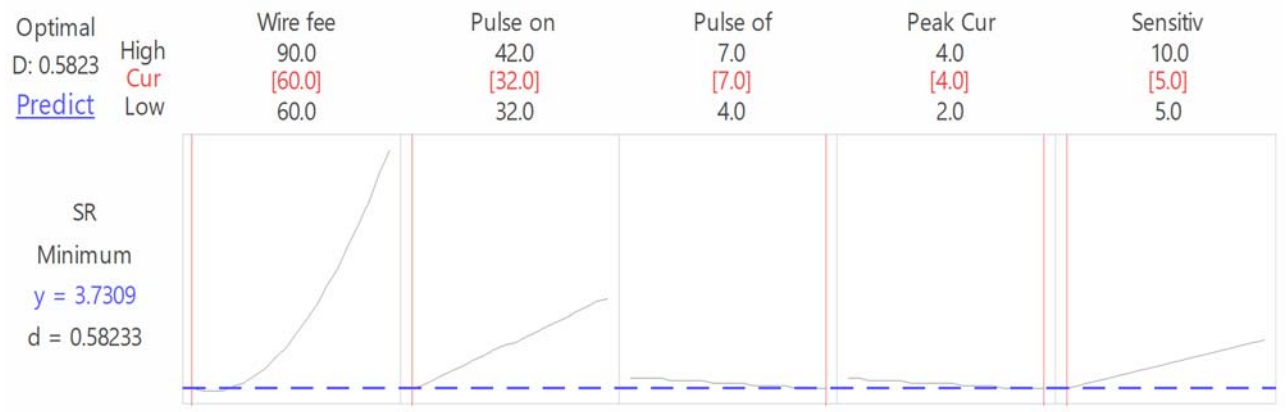

Fig.15. Optimization plot.

The selected wire feed rate (*60 mm/min*) ensures process stability, while a pulse-on time of *32* µ*s* reduces heat input for a finer finish. A pulse-off time of *7* µ*s* aids cooling, minimizing thermal damage and enhancing surface quality. A peak current of *4 A* balances material removal and surface integrity, and a sensitivity setting of *5* improves precision by reducing noise. The design of experiments (DOE) and optimization confirm these settings as effective for minimizing surface roughness. Experimental validation yielded a surface roughness of *3.7309* µ*m*, demonstrating improved performance compared to prior WEDM studies on D2 steel such as Kumar *et al.* [12], who reported comparable values using conventional optimization. These findings confirm the practicality of the selected parameters and underscore the robustness of the proposed optimization framework.

5. Conclusions

In this study, the optimization of WEDM process parameters for D2 steel was carried out using the RSM to minimize the *Ra*. The results demonstrate the significant influence of peak current, pulse on time, and wire feed rate on the surface finish quality. The optimal parameters identified can contribute to improved machining performance and surface integrity in industrial applications involving D2 steel. Materials such as H13 tool steel, Inconel alloys, and titanium, which are commonly used in high-precision industries like aerospace, medical, and automotive, may benefit from a similar approach to optimize their machining

parameters under WEDM or comparable processes. Based on the comprehensive analysis and optimization of the WEDM process parameters, several key conclusions have been drawn.

1. The identified optimal parameter settings for the wire feed rate (*60 mm/min*), pulse on time (*32 μs*), pulse off time (*7 μs*), peak current (*4 A*), and sensitivity (*5*) have proven to be highly effective in minimizing *Ra*.
2. These settings resulted in a *Ra* of approximately *3.7309*, which falls within the desired target range, demonstrating the efficacy of the optimization approach.
3. Each parameter significantly influenced the surface quality. The wire feed rate of *60 mm/min* ensured process stability, while the lower pulse on time (*32 μs*) minimized heat input, yielding a finer surface finish.
4. The extended pulse off time (*7 μs*) allowed for sufficient cooling, reducing thermal damage and enhancing surface quality. The higher peak current (*4 A*) improved material removal rates without compromising surface integrity, and the lower sensitivity (*5*) contributed to greater precision and process stability.
5. The optimization model demonstrated a high degree of reliability, as evidenced by the narrow confidence and prediction intervals for surface roughness. The composite desirability score of *0.582333* further confirms the suitability of these parameter settings. Additionally, the consistency and repeatability of the results were validated by repeated experimental runs under identical conditions, which consistently yielded similar surface roughness values.
6. In practical terms, implementing these optimized settings can significantly improve the surface finish of machined parts, which is especially important in applications where surface quality is critical. Moreover, this study underscores the importance of carefully balancing process parameters to achieve the desired outcomes efficiently, thus enhancing the overall efficiency and quality of manufacturing operations.

6. Future work

1. To improve industrial applicability, future work should extend the current experimental and statistical methodology to a wider range of materials.
2. Exploring WEDM optimization for materials like H13 tool steel, Inconel 718, and titanium alloys would demonstrate the approach's versatility and reveal material-specific sensitivities, supporting the development of adaptable machining strategies.
3. Incorporating additional responses such as material removal rate, wire wear ratio, and recast layer thickness can enhance understanding of both performance and surface integrity across various materials.
4. Employing advanced or hybrid optimization methods such as RSM, GRA, Genetic Algorithm, or PSO could improve multi-response optimization and parameter interaction modeling, leading to higher desirability scores.
5. Future studies should also integrate economic and sustainability considerations (e.g., machining time, tool wear, energy consumption) within a multi-objective optimization framework to better balance surface quality with operational efficiency.
6. Investigating process stability through key factors like wire breakage, electrode wear, and residual stresses using tools such as high-speed imaging, SEM, and XRD will provide deeper insight into reliability and support robust parameter refinement for industrial deployment.

Nomenclature

WEDM – Wire Electrical Discharge Machining
RSM – Response Surface Methodology
CCD – Central Composite Design
Ra – surface roughness
ANOVA – Analysis of Variance

MRR – material removal rate
ANN – Artificial Neural Network
PSO – particle swarm optimization
TLBO – Teaching Learning Based Optimization
GRA – Grey relational analysis
CNC – Computer Numerical Control
DOE – Design of Experiment

References

[1] Arunadevi M. and Prakash C.P.S. (2021): *Predictive analysis and multi objective optimization of wire-EDM process using ANN*.– Mater. Today: Proc., vol.46, pp.6012-6016.

[2] Arya R. and Singh H. (2022): *Optimization of Wire-cut EDM process parameters using TLBO algorithm*.– Eng. Res. Express, vol.4, No.3, pp.035051.

[3] Ay M. and Etyemez A. (2020): *Optimization of the effects of wire EDM parameters on tolerances*.– Emerg. Mater. Res., vol.9, No.2, pp.527-531.

[4] Babu B.S., Sathiyaraj S., Ramesh A.K.P., Afridi B.A. and Varghese K.K. (2021): *Investigation of machining characteristics of aluminium 6061 by wire cut EDM process*.– Mater. Today: Proc., vol.45, pp.6247-6252.

[5] Babu K.N., Karthikeyan R. and Punitha A. (2019): *An integrated ANN-PSO approach to optimize the material removal rate and surface roughness of wire cut EDM on INCONEL 750*.– Mater. Today: Proc., vol.19, pp.501-505.

[6] Bhatt D. and Goyal A. (2019): *Multi-objective optimization of machining parameters in wire EDM for AISI-304*.– Mater. Today: Proc., vol.18, pp.4227-4242.

[7] Camposeco-Negrete C. (2019): *Prediction and optimization of machining time and surface roughness of AISI O1 tool steel in wire-cut EDM using robust design and desirability approach*.– Int. J. Adv. Manuf. Technol., vol.103, pp.2411-2422.

[8] Camposeco-Negrete C. (2021): *Analysis and optimization of sustainable machining of AISI O1 tool steel by the wire-EDM process*.– Adv. Manuf., vol.9, No.2, pp.304-317.

[9] Devarasiddappa D. and Chandrasekaran M. (2020): *Experimental investigation and optimization of sustainable performance measures during wire-cut EDM of Ti-6Al-4V alloy employing preference-based TLBO algorithm*.– Mater. Manuf. Process., vol.35, No.11, pp.1204-1213.

[10] Divya M., Sateesh N. and Subbiah R. (2020): *Review on multi objective optimization of wire cut EDM process parameters using grey relational analysis*.– Mater. Today: Proc., vol.26, pp.3124-3130.

[11] Gnanavelbabu A., Saravanan P., Rajkumar K., Karthikeyan S. and Baskaran R. (2018): *Optimization of WEDM process parameters on multiple responses in cutting of Ti-6Al-4V*.– Mater. Today: Proc., vol.5, No.13, pp.27072-27080.

[12] Kumar A., Jagota V., Shawl R.Q., Sharma V., Sargam K., Shabaz M. and Gandhi S. (2021): *Wire EDM process parameter optimization for D2 steel*.– Mater. Today: Proc., vol.37, pp.2478-2482.

[13] Kumar A., Soota T. and Kumar J. (2018): *Optimisation of wire-cut EDM process parameter by Grey-based response surface methodology*.– J. Ind. Eng. Int., vol.14, pp.821-829.

[14] Marelli D., Singh S.K., Nagari S. and Subbiah R. (2020): *Optimisation of machining parameters of wire-cut EDM on super alloy materials - a review*.– Mater. Today: Proc., vol.26, pp.1021-1027.

[15] Mohamed M.F. and Lenin K. (2020): *Optimization of Wire EDM process parameters using Taguchi technique*.– Mater. Today: Proc., vol.21, pp.527-530.

[16] Natarajan E., Kaviarasan V., Lim W.H., Ramesh S., Palanikumar K., Sekar T. and Mok V.H. (2022): *Gorilla troops optimizer combined with ANFIS for wire cut EDM of aluminum alloy*.– Adv. Mater. Sci. Eng., vol.2022, No.1, pp.3072663.

[17] Natarajan K., Ramakrishnan H., Gacem A., Vijayan V., Karthiga K., Ali H.E. and Mekonnen A. (2022): *Study on optimization of WEDM process parameters on stainless steel*.– J. Nanomater., vol.2022, No.1, pp.6765721.

[18] Praveen D.V., Raju D.R. and Raju M.J. (2020): *Optimization of machining parameters of wire-cut EDM on ceramic particles reinforced Al-metal matrix composites - a review*.– Mater. Today: Proc., vol.23, pp.495-498.

[19] Ramanan G. and Dhas J.E.R. (2018): *Multi objective optimization of wire EDM machining parameters for AA7075-PAC composite using grey-fuzzy technique*.– Mater. Today: Proc., vol.5, No.2, pp.8280-8289.

[20] Reddy M.C., Rao K.V. and Suresh G. (2021): *An experimental investigation and optimization of energy consumption and surface defects in wire cut electric discharge machining*.– J. Alloys Compd., vol.861, pp.158582.

[21] Sampath B., Myilsamy S. and Sukkasamy S. (2021): *Experimental investigation and multi-objective optimization of cryogenically cooled near-dry wire-cut EDM using TOPSIS technique*.– Preprint, Research Square, https://doi.org/10.21203/rs.3.rs-254117/v1.

[22] Selvam R., Vignesh M., Pugazhenthi R., Anbuchezhiyan G. and Satyanarayana Gupta M. (2024): *Effect of process parameter on wire cut EDM using RSM method*.– Int. J. Interact. Des. Manuf. (IJIDeM), vol.18, No.5, pp.2957-2968.

[23] Sen B., Dasgupta A. and Bhowmik A. (2024): *Optimizing wire-cut EDM parameters through evolutionary algorithm: A study for improving cost efficiency in turbo-machinery manufacturing*.– Int. J. Interact. Des. Manuf. (IJIDeM), pp.1-12.

[24] Seshaiah S., Sampathkumar D., Mariappan M., Mohankumar A., Balachandran G., Kaliyamoorthy M. and Gopal R. (2022): *Optimization on material removal rate and surface roughness of stainless steel 304 wire cut EDM by response surface methodology*.– Adv. Mater. Sci. Eng., vol.2022, No.1, pp.6022550.

[25] Subrahmanyam M. and Nancharaiah T. (2020): *Optimization of process parameters in wire-cut EDM of Inconel 625 using Taguchi's approach*.– Mater. Today: Proc., vol.23, 642-646.

[26] Tata N., Pacharu R.K. and Devarakonda S.K. (2021): *Multi response optimization of process parameters in wire-cut EDM on INCONEL 625*.– Mater. Today: Proc., vol.47, pp.6960-6964.

[27] Wasif M., Khan Y.A., Zulqarnain A. and Iqbal S.A. (2022): *Analysis and optimization of wire electro-discharge machining process parameters for the efficient cutting of aluminum 5454 alloy*.– Alexandria Eng. J., vol.61, No.8, pp.6191-6203.

[28] Wang T., Wang L., Liu S., Chen L., Jin X., Liu H. and Liao X. (2025). *The in situ green synthesis of metal organic framework (HKUST-1)/cellulose/chitosan composite aerogel (CSGA/HKUST-1) and its adsorption on tetracycline*.– Nordic Pulp & Paper Research Journal, vol.40, No.1, pp.219-233.

[29] Nguyen-Ngoc L., Nguyen-Huu Q., De Roeck G., Bui-Tien T. and Abdel-Wahab M. (2024). *Deep neural network and evolved optimization algorithm for damage assessment in a truss bridge*.– Mathematics, vol.12, No.15, pp.2300.

[30] Bai J., Nguyen-Xuan H., Atroshchenko E., Kosec G., Wang L. and Wahab M.A. (2024). *Blood-sucking leech optimizer*.– Advances in Engineering Software, vol.195, pp.103696.

[31] Qin S., Feng J., Tang J., Huo X., Zhou Y., Yang F. and Wahab M.A. (2024). *Condition assessment of a concrete filled steel tube arch bridge using in-situ vibration measurements and an Improved Artificial Fish Swarm Algorithm*.– Computers & Structures, vol.291, pp.107213.

[32] Li Y., Minh H.L., Cao M., Qian X. and Wahab M.A. (2024). *An integrated surrogate model-driven and improved termite life cycle optimizer for damage identification in dams*.– Mechanical Systems and Signal Processing, vol.208, pp.110986.

[33] Khandan A., Abdellahi M., Ozada N. and Ghayour H. (2016). *Study of the bioactivity, wettability and hardness behaviour of the bovine hydroxyapatite-diopside bio-nanocomposite coating*.– Journal of the Taiwan Institute of Chemical Engineers, vol.60, pp.538-546.

[34] Khandan A., Abdellahi M., Barenji R.V., Ozada N. and Karamian E. (2015). *Introducing natural hydroxyapatite-diopside (NHA-Di) nano-bioceramic coating*.– Ceramics International, vol.41, No.9, pp.12355-12363.

[35] Karamian E., Abdellahi M., Khandan A. and Abdellah S. (2016). *Introducing the fluorine doped natural hydroxyapatite-titania nanobiocomposite ceramic*.– Journal of Alloys and Compounds, vol.679, pp.375-383.

[36] Karimi M., Asefnejad A., Aflaki D., Surendar A., Baharifar H., Saber-Samandari S., Khandan A., Khan A. and Toghraie D. (2021). *Fabrication of shapeless scaffolds reinforced with baghdadite-magnetite nanoparticles using a 3D printer and freeze-drying technique*.– Journal of Materials Research and Technology, vol.14, pp.3070-3079.

[37] Liang H., Mirinejad M.S., Asefnejad A., Baharifar H., Li X., Saber-Samandari S., Toghraie D. and Khandan A. (2022).– *Fabrication of tragacanthin gum-carboxymethyl chitosan bio-nanocomposite wound dressing with silver-titanium nanoparticles using freeze-drying method*.– Materials Chemistry and Physics, vol.279, pp.125770.

[38] Deshmukh D.D. and Kharche Y. (2023). *Influence of processing conditions on the tensile strength and failure pattern of resistance spot welded SS 316L sheet joint*.– International Journal on Interactive Design and Manufacturing (IJIDeM), pp.1-13.

[39] Deshmukh D.D. and Kalyankar V.D. (2021). *Analysis of deposition efficiency and distortion during multitrack overlay by plasma transferred arc welding of Co-Cr alloy on 316L stainless steel*.– Journal of Advanced Manufacturing Systems, vol.20, No.4, pp.705-728.

[40] Deshmukh D.D. and Kalyankar V.D. (2019). *Deposition characteristics of multitrack overlay by plasma transferred arc welding on SS316L with Co-Cr based alloy-influence of process parameters*.– High Temperature Materials and Processes, vol.38, No.2019, pp.248-263.

[41] Deshmukh D., Kakade S., Kabudke P., Mhaske M. and Dond D. (2024): *Investigations on hardfacing characteristics of Ni-based alloy on Ass 304 using plasma transferred arc welding at different speeds*.– International Journal of Modern Manufacturing Technologies (IJMMT), vol.16, No.2, pp.32-40, DOI:10.54684/ijmmt.2024.16.2.32.

[42] Wagh S.V., Jagtap S.G., Sable M.J. and Deshmukh D. (2025): *Metallurgical characterization of Cr2O3 and Al2O3 coatings on SS 316L: implications for durability in desalination environments*.– Transactions of the Indian Institute of Metals, vol.78, No.3, pp.1-14.

[43] Bhoskar A., Naik H., Kalyankar V. and Deshmukh D. (2025). *Nickel-based metallurgical coating architectures for superior wear resistance in high-temperature P91 steel applications*.– Journal of Alloys and Metallurgical Systems, vol.9, pp.100151.

[44] Kalyankar V., Bhoskar A., Deshmukh D. and Patil S. (2022): *On the performance of metallurgical behaviour of Stellite 6 cladding deposited on SS316L substrate with PTAW process*.– Canadian Metallurgical Quarterly, vol.61, No.2, pp.130-144.

[45] Bhoskar A., Kalyankar V. and Deshmukh D. (2023). *Metallurgical characterisation of multi-track Stellite 6 coating on SS316L substrate*.– Canadian Metallurgical Quarterly, vol.62, No.4, pp.665-677.

[46] Kakade S.P., Thakur A.G., Deshmukh D.D. and Patil S.B. (2023): *Experimental investigations and optimisation of Ni-Cr-B-Si hardfacing characteristics deposited by PTAW process on SS 410 using response surface method*.– Advances in Materials and Processing Technologies, vol.9, No.3, pp.826-842.

[47] Bhoskar A., Kalyankar V. and Deshmukh D. (2024). *Implications of FCC and HCP cobalt phases on wear performance of weld deposited cobalt-based coating*.– Results in Surfaces and Interfaces, pp.100247.

[48] Qin W., Kolooshani A., Kolahdooz A., Saber-Samandari S., Khazaei S., Khandan A., Ren F. and Toghraie D. (2021). *Coating the magnesium implants with reinforced nanocomposite nanoparticles for use in orthopedic applications*.– Colloids and Surfaces A: Physicochemical and Engineering Aspects, vol.621, pp.126581.

Received: March 5, 2025
Revised: September 11, 2025